New insights in the adsorption behavior of triethanolamine on OPC by experimental and theoretical study

Qi Zhai[a, d], Kiyofumi Kurumisawa[b, *], Hegoi Manzano[c], Juhyuk Moon[d], In-Hee Hwang [e]

[a] Division of Sustainable Resources Engineering, Graduate School of Engineering, Hokkaido University, Japan

[b] Division of Sustainable Resources Engineering, Faculty of Engineering, Hokkaido University, Japan

[c] Departamento de FÃsica, Facultad de Ciencia y TecnologÃa Universidad del PaÃs Vasco UPV/EHU, Barrio Sarriena s/n, Leioa, 48940, Bizkaia, Spain

[d] Department of Civil and Environmental Engineering, Seoul National University, Korea

[e] Division of Environmental Engineering, Faculty of Engineering, Hokkaido University, Japan

***Correspondence:**

Kiyofumi Kurumisawa

Full postal address:

Email:

Abstract

The influence of triethanolamine (TEA) on the hydration of cement-based materials is closely linked to its adsorption behavior in Ordinary Portland Cement (OPC). This study investigated the adsorption process and mechanism of TEA on OPC and pure mineral phases—alite, gypsum, aluminate+gypsum, and calcium hydroxide (CH)—in the first 8 h. The results revealed that in all single phases, TEA adsorption was associated with alite and CH. The crystal structure of CH did not change during adsorption, likely due to the physical adsorption of TEA. During OPC hydration, the adsorption of TEA was primarily associated with the hydration of alite. In the initial hydration stage, only CH served as the main adsorption receptor, which was supported by adsorption energy simulations using molecular dynamics. As alite hydration progresses, the role of the receptor may shift toward calcium silicate hydrate (C-S-H), as indicated by the calculated adsorption limit of CH. Furthermore, density functional theory (DFT) demonstrated that TEA-Ca^{2+} has

the lowest complexation energy when the ligand-to-metal ratio is 1:1 and becomes even more stable when the ligand-to-metal ratio is 2:1.

Keywords: triethanolamine; adsorption; sustainability; molecular dynamics simulation; DFT simulation.

1. Introduction

Cement additives play a significant role in reducing the environmental impacts associated with cement production. Triethanolamine (TEA) has been extensively studied as a cement-grinding agent and performance enhancer for a considerable period [1,2]. TEA can act as an effective dispersant in the cement grinding process. It can also prevent powder agglomeration, which leads to improved grinding outcomes owing to its inherently organic polar nature [3]. The addition of TEA is associated with a lower angle of repose of the ground cement, which, subsequently enhances flowability [4]. Jachiet et al. [5] suggested that TEA promotes the dispersion of cement particles, attributed to the repulsive depletion forces induced by TEA. Additionally, Mishra et al. [6] explained TEA's effectiveness as a grinding agent through molecular dynamics (MD) simulations, thereby highlighting how TEA's Coulomb interactions between cleaved clinker surfaces reduce agglomeration.

However, numerous studies have indicated that TEA, beyond its grinding-enhancing properties, can alter the particle size distribution during grinding and potentially influence the hydration and mechanical performance of ordinary Portland cement (OPC) [4,7,8]. With the increasing focus on low-carbon construction materials, TEA has gained popularity as a performance enhancer owing to its high effectiveness at relatively low dosages [9,10]. The influence of TEA on OPC hydration is attributed to the complex formed between TEA and alkali metal ions via complexation [11–14]. For instance, the complex between Ca^{2+} and TEA can affect the concentration of Ca^{2+} in the solution, which subsequently affect the hydration of alite (C_3S) [15]. Using density functional theory (DFT), Yaphary et al. [16] suggested that TEA complexes with Al^{3+} act as electron-pair donors to accelerate the hydration of tricalcium aluminate (C_3A).

It is widely acknowledged that TEA's effects on OPC are dose-dependent, potentially disrupting the balance between the hydration rates of aluminate and alite [17,18]. High dosages of TEA (> 0.1% wt of OPC) have been shown to control OPC hydration through C_3A and ferrite (C_4AF) hydration. This results in significant ettringite (AFt) precipitation, which can cause undersulfation [15]. This can accelerate renewed C_3A hydration and strongly inhibit the main hydration of C_3S [19,20], thereby resulting in flashing setting, stiffening, and reduced workability [10,16]. However, within an appropriate dosage range, TEA has been found to promote OPC hydration and increase early-age mechanical properties [21–23].

The dual functions of TEA as an agent and additive have been extensively studied. Moreover, adsorption is a common phenomenon that exists across both functions. Significant decreases in TEA concentration in the pore solutions of OPC, as observed by total organic carbon (TOC) analysis, suggest adsorption onto surfaces including C_3S, C_3A, calcium-silicate-hydrate (C-S-H), calcium hydroxide (CH), or other minerals [19,24]. This possibly explains why TEA is effective mainly at early ages [22]. This adsorption is believed to be driven by Ca complexation, hydrogen bonding, and other polar interactions with the clinker surfaces or hydration products [6,25]. Adsorption of TEA has also been observed in several systems. The adsorption of the TEA-Ca^{2+} complex on the surface of CH, which inhibits its growth, is a frequently mentioned phenomenon [12,26,27]. The adsorption of TEA onto the surface of C_3S in single or OPC systems has also been reported [6,11,24]. Yaphary et al. [40] suggested that the growth of the TEA-AFt complex on C_3A surfaces and partly on C_3S surfaces slows the formation of C-S-H.

Conversely, Jachiet et al. [5] observed no TEA adsorption after 10 min of hydration, suggesting that TEA may not exhibit electrostatic or steric effects, which contradicts previous results. This highlights the ongoing controversy regarding whether TEA absorbs within OPC systems and, if so, on which specific mineral surfaces. Despite extensive research on TEA’s adsorption effects on individual clinker or OPC systems, no study has comprehensively addressed these problems or explicitly linked them to the hydration processes in OPC.

Understanding the adsorption behavior is essential for comprehending the performance of TEA in OPC and cementitious materials. This study aims to systematically clarify the adsorption process and mechanism of TEA onto OPC. Various systems including OPC,

C_3S, Gypsum+C_3A, Gypsum, and CH were investigated because of the complexity of OPC. C_4AF and belite (C_2S) were not considered because of their low reactivity during the initial stage. The adsorption experiments were characterized using TOC content measurements, X-ray diffraction (XRD), thermogravimetric analysis (TG), and isothermal calorimetry. The mechanism was further elucidated using MD and density functional theory (DFT) simulations.

2. Methodology

2.1. Materials

The OPC used in the study was supplied by Nippon Steel (Hokkaido, Japan). Given that the primary C_3S in the OPC used was in monoclinic form, pure C_3S-M3, and cubic C_3A sourced from Hunan Scientific Research Tree Technology Service Co., Ltd. were used. Moreover, reagent-grade CH, gypsum, and TEA (99.3%) were obtained from Kanto Chemical Co. Inc. Chemical composition tests were conducted in accordance with JIS R 5202 and JIS R 5204, and the crystal compositions of the clinkers were analyzed using X-ray fluorescence (XRF, JSX3100R) and X-ray diffraction (XRD, MultiFlex), as detailed in Table 1 and Fig. 1.

Table 1
Chemical composition of materials (mass%).

Component	C_3S	C_3A	OPC	Mineralogical Composition of OPC	
SO_3	0.59	0.17	1.50	C_3S	53.5
SiO_2	26.36	0.19	20.48	C_2S	9.07
TiO_2	-	0.03	0.29	C_3A	7.52
Al_2O_3	0.30	36.76	5.06	C_4AF	9.33
Fe_2O_3	3.90	3.77	2.89	Bassanite	3.74
MnO	0.06	0.07	0.05	Calcite	4.32
MgO	0.59	0.17	1.50		
CaO	68.34	58.58	66.88		
Na_2O	-	-	0.22		
K_2O	0.45	0.34	0.27		

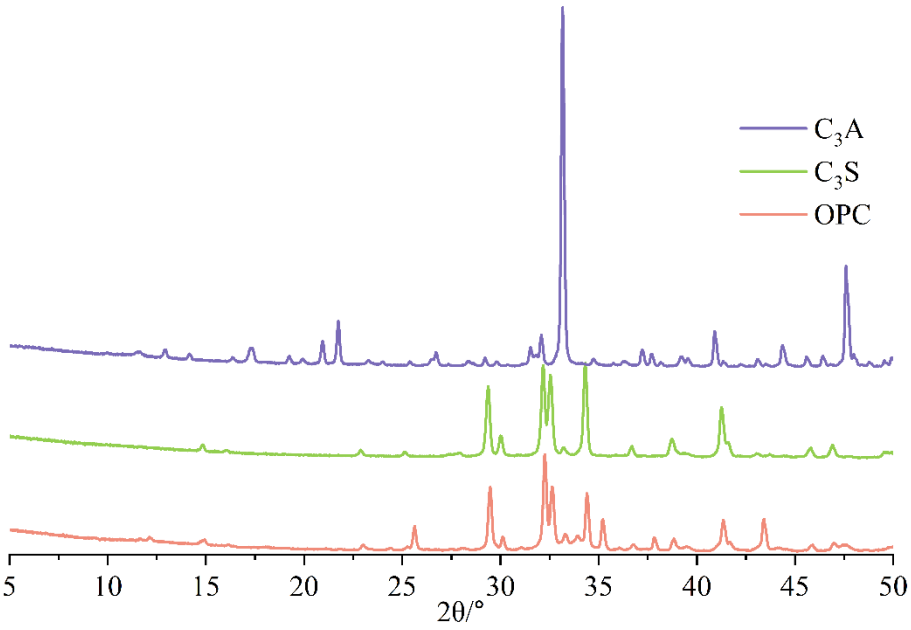

2.2.Experiment

2.2.1. binder preparation

This study aims to detect the adsorption of TEA during hydration. Distilled water was used as the control. A typical dosage of 0.05%, which is commonly used in practice, and a significantly higher dosage of 0.5% by weight of OPC were used in this study. Several factors led to the selection of the water-to-binder (w/b) ratio. Initially, higher w/b ratios typically used for adsorption, such as 1:100 and 1:1000, were considered. However, at 0.5% TEA, changes in concentration could not be detected. Therefore, we selected w/b ratios within the normal range to prepare the cement paste. To prepare the pore solution, a slightly higher w/b ratio (0.6 was used for the OPC, C_3S, the C_3A/Gypsum binder, and gypsum [28]. Owing to the low solubility of portlandite, the w/b ratio was set to two. To prevent the flash setting of C_3A alone, 20% gypsum was mixed with C_3A. To facilitate accurate comparison of TEA adsorption, evaluating the remaining TEA concentration in the solution is imperative. Thus, selecting an appropriate reference standard is critical. Owing to variations in water–cement ratios, using the percentage of solid substance as the standard, such as determining the amount of TEA added to the system at 0.05% wt, inevitably results in different TEA concentrations across systems. Consequently, we standardized by maintaining a consistent TEA concentration across all systems. For

clarity in subsequent sections, 0.05% and 0.5% TEA solutions are referred to as 830 ppm and 8300 ppm, respectively.

2.2.2. Adsorption experiment

The binder was mixed with varying dosages of TEA solution and filled into 50 ml centrifuge tubes. The tubes were agitated at 260 rpm using an eight-type shaker (YAYOI, 8-20-w) for 2 min, 1, 3, 6, and 8 h. Upon reaching a specified age, the samples were centrifugation at 9000rpm for 4 min. The supernatant was carefully collected and filtered through a 0.45μm syringe filter. The resulting filtrate was diluted with deionized water to ratios of 1:100 and 1:1000. Subsequently, the solutions were promptly analyzed using a TOC analyzer (Shimadzu, TOC-V) in TC mode. Potassium hydrogen phthalate and sodium hydrogen carbonate were used as standard solutions for total carbon (TC) and inorganic carbon (IC), respectively. The organic carbon (OC) content and TEA concentration in the pore solution were calculated as follows:

$$OC = (TC - IC) * f \quad (1)$$

$$C_{TEA} = OC * 149.19/72 \quad (2)$$

where *f* represents the corresponding dilution times.

2.2.3. Calorimetric measurements

To establish the intrinsic connection between adsorption behavior and hydration, the heat of hydration was determined for binders of C_3S, C_3A+gypsum, and OPC using a microcalorimeter (MMC-5116, Tokyo Riko). To ensure homogeneity, the powder and solution were manually stirred in a beaker for 5 min before being transferred to an ampoule. Furthermore, to address environmental condition disparities between the interior and exterior of the machine, the exothermic heat within the first hour was excluded to ensure stability.

2.2.4. Phase assemblage after adsorption

The solid residues obtained after centrifugation were collected for further analysis to investigate the influence of adsorption on the phase transformation. Given the initial sensitivity of paste hydration, various hydration stoppage methods were compared, as detailed in the Supplementary Materials. After comparison, the collected solids underwent hydration stoppage by immersion in acetone for 1 h, followed by drying at

40°C for one day. Subsequently, the solids were ground into powder using an agate mortar and sieved through a screen with a size of less than 300 μm for powder XRD and thermogravimetric (TG) analysis. For the powder XRD analysis, the sample was mixed with 20% corundum powder, which served as an internal standard. Measurements were conducted using a MultiFlex diffractometer (Cu-Kα, 40 kV, 40mA) with 1° axial Soller slits. The instrument operated in step-scan mode, scanning between 5° and 70° (2θ) with a step size of 0.01° (2θ) for 0.6 seconds per step. Phase identification and quantitative analysis were performed using the Profex software [29]. The CH content was further confirmed through TG using a Hitachi TG7000 instrument. Approximately 10 mg of the powder was placed in a platinum pan and equilibrated at 20°C. The heating rate was set at 10°C/min from 20 to 1000°C under a nitrogen (N_2) gas atmosphere. The CH content was calculated based on the mass loss in the temperature range between 450°C to 550°C using the tangent method. Additionally, the CH content was cross-referenced with anhydrous pastes using loss-on-ignition (LOI) analysis (JIS R 5202), with the detailed experimental procedures explained in [30,31]. Additionally, in situ, XRD analysis was conducted to qualitatively analyze the impact of the adsorption behavior on the crystal structure of portlandite without the influence of hydration stoppage. Similar to the calorimetric measurements, the samples were manually mixed and transferred to a custom sample holder with a non-diffracting plate. The sample was covered with a Kapton film to prevent carbonation and evaporation during the analysis. The in-situ XRD measurements were carried out using 1/2° axial Soller slits, scanning between 5° and 50° (2θ) with a step size of 0.01° (2θ) for 0.6 seconds per step. This method allowed for the real-time observation of any changes in the crystal structure of portlandite during the experiment. In addition, thermodynamic modeling was employed to verify the degree of hydration of OPC and the measured CH content. modeling was conducted using GEM-Selektor version 3 [32] (GEMS) in conjunction with the aqueous species database from PSI-GEMS and cement minerals included in the cemdata18 [33]. Thermodynamic modeling of the hydration of OPC followed a method similar to that described in[34].

2.2.5. Molecular simulations

The role of the intercalated TEA was investigated using molecular simulations to elucidate the interfacial interaction mechanisms between TEA and OPC components. The

INTERFACE force field (IFF) was used for the inorganic materials, in combination with the PCFF with the 9-6 form of the LJ potential for the organic molecules and the SPC-like water model. This combination has been previously used in the investigation of organic and inorganic interactions [35] and has been proven to be suitable for modeling the interactions of organic modifiers with all major phases in cement [6,25,36]. The construction of the solid-organic interface followed the methodology of Mishra and Heinz, where the interaction surfaces of Gypsum [37], C_3A [25], C_3S [6,38,39], and CH [40] were selected based on the minimal cleavage energy. Notably, the (040) surface of M3-C_3S was selected due to its low cleavage energy, with the [010] direction indicating the plane orientation [38,39]. The force-field parameters used in this study can be found in [6,25,35,36]. In all simulations, the surface dimensions were at least 2.4*2.5 nm, and the slab thickness was > 2 nm. A vacuum slab > 12 nm was set, and assuming a solution density of 1g/cm^3, 4000 water molecules were added to keep the water layer as thick as possible to avoid any surface-surface interactions due to periodic boundary conditions. The total height of the simulation boxes was determined by the base height of the solid component and additive molecular volumes for simulating the high dosage of 8300 ppm used in the experiment, 4 molecules of TEA were introduced. The simulations were performed using LAMMPS [41]. The TEA molecules were initially positioned 0.5 nm near the surface of the minerals. Energy minimization was used to relax the initial configurations, followed by a 1 ns equilibration of water in the canonical (NVT) ensemble at a temperature of 298.15 K. Subsequently, molecular dynamics simulations were conducted using an isothermal isobaric (NPT) ensemble at 101 kPa for 1 ns to optimize the molecular volumes and maintain an average pressure tensor close to the standard pressure [42]. The system was further simulated under the NVT ensemble at a temperature of 298.15 K with a time step of 1 fs, a spherical cutoff for van der Waals interactions of 1.2 nm. The total simulation time was 5 ns, with 4 ns of pre-equilibration and 1 ns for collecting the thermodynamic data. For each system, three simulations were performed using independent start structures.

2.2.6. Stability constant of the complex between triethanolamine and metal ions

Density functional theory (DFT) results were obtained through geometry optimization and frequency analysis using the Gaussian 16. To compare the complexation abilities

between TEA with metal ions (Ca, Mg, Al, and Na) side by side, ωB97XD exchange-correlation functional, in conjunction with 6-311 G** basis set, was selected for geometry optimization. The solvation effects were accounted for by considering the optimized gas-phase structures in an aqueous medium using a polarizable continuum model (PCM) [43]. Vibrational frequency calculations were performed on the optimized structures to confirm their stable configurations, and no negative frequencies were observed. Highly accurate single-point energies were obtained using the M06-2X functional combined with an all-electron higher-level def2-TZVPP basis set, and the solvation model density (SMD) (water as the solvent) was used to calculate complex energies based on the optimized structures [44]. These two functionals are effective for the structural optimization of systems involving main-group elements [45].

Free energies were evaluated by summing the electron energies and thermal corrections to free energy obtained by frequency analysis at ωB97XD/6-311 G** level using the Shermo 2.6 software [46]. Considering that no scale factor is available for zero-point energy (ZPE) at this level, a scale factor of 1.028 was determined using a method similar to that proposed in [47] Details of this method are provided in the supplementary data. Electronic structure analyses were conducted using the Multiwfn program [48], and isosurface maps were visualized using the Visual Molecular Dynamics (VMD) software [49].

3. Results and discussion

3.1.Adsorptive properties of triethanolamine on minerals

The adsorption behavior of TEA on different minerals was also investigated. Fig.2 shows the change in TEA concentration of TEA mixed with various minerals over time. Concentration changes in the graphs are shown primarily as relative values, that is, the rate of change in TEA concentration, to minimize errors caused by background changes during each measurement.

Typically, an increase in the TEA concentration was observed in most minerals at 2 min, regardless of the dosage. This phenomenon can be partly explained by the initial use of mill crushing to obtain C_3A, C_3S, and OPC with the addition of a milling agent. Powder

dispersion and dissolution during initial hydration may have caused some of the agents to dissolve in the solution [5]. Similar increases in the alkanolamine concentration in solution during the early stages of hydration have been reported in previous studies [19,26]. As the specific type of this agent was unknown, the concentration of organic carbon in the control group was measured over time (Fig.2(c)). However, the change in this concentration was not constant, preventing it from being directly deduced as the background. Nevertheless, it was observed that the organic content of the fraction was consistently in the range of -80 to 150 ppm, which would not significantly affect the overall trend.

Overall, it can be inferred that the adsorption behavior was not related to the unhydrated raw OPC, C_3S, or C_3A, as no decrease in the tendency was observed before 1 h in either case. The relationship of gypsum and C_3A+gypsum with TEA adsorption was not significant at either dosage. The TEA concentration in the C_3A+gypsum binder tended to increase regardless of the TEA dosage. This phenomenon may be linked to the hydration of C_3A by gypsum, as reported by Quennoz et al. [50]. They noted that a solid solution of hydroxy-AFm, SO_4-AFm, and even hemicarboaluminate (Hc) forms early in hydration when 20% gypsum is present. The formation of HC could potentially overestimate the total carbon amount owing to an increase in inorganic carbon. However, notable correlation occurred between TEA adsorption and CH. When CH contacted TEA, the TEA concentration in the solution decreased drastically, particularly at 830 ppm, where nearly all the TEA was adsorbed. At 8300 ppm, although the TEA concentration initially decreased sharply, the trend stabilized after 3 h, indicating a likely upper limit of CH adsorption. The adsorption behavior of TEA was also correlated with the hydration of OPC and C_3S. As OPC and C_3S were hydrated, the amount of TEA decreased. The adsorption curves of OPC and C_3S exhibit striking similarities at 830 ppm. Initially, there was an insignificant change in the TEA concentration in the first 3 h, followed by a sharp decrease. However, at 8300 ppm, the trends differed significantly. Both OPC and C_3S showed insignificant changes in the TEA concentration in the first 3 h. However, after 3 h, the TEA concentration in the C_3S solution decreased sharply, whereas in the OPC solution, it remained unchanged or even increased. Several hypotheses have been proposed based on the adsorption experiments.

1. The adsorption behavior of TEA in cement materials is strongly related to cement hydration, particularly the production pathway of CH during early hydration. It indicates a close relationship between TEA adsorption and C_3S hydration.

2. The TEA adsorption behavior closely aligns with the TEA dosage, as evidenced by the potential upper limit of adsorption at high dosages, which may also impact cement hydration.

These hypotheses will be further verified in subsequent sections of the study.

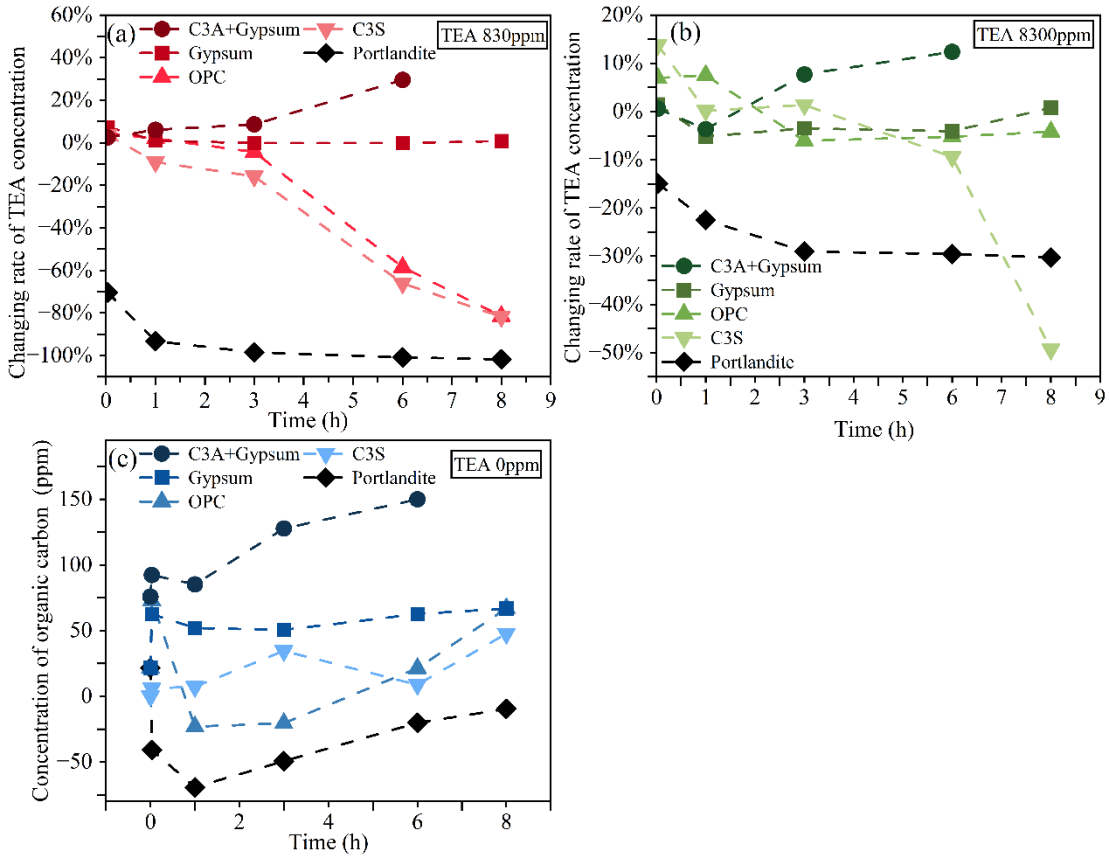

Fig.2. Evolution of TEA adsorption behavior over time at different dosages: (a) 830 ppm, (b) 8300 ppm, and (c) 0 ppm.

3.2.Analysis of the isothermal calorimetric measurements

The effect of TEA on cement hydration kinetics was investigated to further illustrate the relationship between cement hydration and TEA adsorption behavior. Fig.3 shows the initial hydration of the cementitious binders with and without TEA. In OPC with 830 ppm of TEA, the initial hydration was inhibited to some extent (Fig. 3 (a) and (b)), which aligned with the observed retarding effect in pure C_3S (Fig. 3(c) and (d)). However, in the

presence of 8300 ppm TEA, although the hydration of C_3S was initially retarded before 6 h, rapid hydration was observed, as shown in Fig. 3(d). Conversely, in OPC, a pronounced retardation effect on the hydration of C_3S was observed, in which the main reaction of C_3S, which was expected to occur in OPC, did not occur during the initial stages of hydration. While a rapid cumulative heat generation was observed before 8 hours, the sharp exothermic peak corresponded to the initial hydration of C_3A [19], and after 8 hours, it appears that the hydration process came to a standstill. Fig. 3(e) and (f) also show enhanced C_3A reaction with the addition of TEA. This indicates that the hydration of C_3S in OPC systems with high TEA dosages is complex. However, in pure C_3S hydration, TEA may directly retard the hydration of C_3S by the formation of the TEA-Ca^{2+} complex layer [26], and more attention should be paid to the interaction of aluminate and silicate reactions in OPC systems. For example, Juilland et al. [51] The most significant difference between these two systems is the presence of rapidly soluble alkali-metal salts.

The influence of TEA on the hydration process was consistent with its adsorption behavior. First, it can be confirmed that the hydration of C_3A shows no significant relationship with the adsorption of TEA in the C_3A+gypsum and OPC systems because the reaction of C_3A was not hindered by the addition of TEA and was even promoted. Accordingly, the formation of AFm-like phases and AFt also revealed no significant relationship with the adsorption of TEA. While some previous studies posited that the accelerated aluminate reaction was caused by the adsorption of TEA-AFt complexes and that the hydration phase, such as AFm precipitated by the accelerated aluminate reaction, can consume a large amount of TEA [16,19]. In an investigation conducted by Gartner et al. [52], it was suggested that TEA may be adsorbed onto the AFm surface during the hydration of C_4AF in the presence of gypsum and portlandite, as evidenced by a decrease in TEA concentration in lime-gypsum and cement solutions. However, the potential role of CH, which could be a key factor in this process, may have been overlooked.

The similar hydration tendencies of OPC and C_3S with 830ppm TEA exhibit a good correlation with the adsorption curves. However, in the presence of 8300ppm TEA, with a lack of hydration of C_3S, no adsorption was observed in the OPC system. In pure C_3S systems, delayed hydration corresponds to delayed adsorption phenomenon as well. This further justifies the assumptions made in Section 3.1.

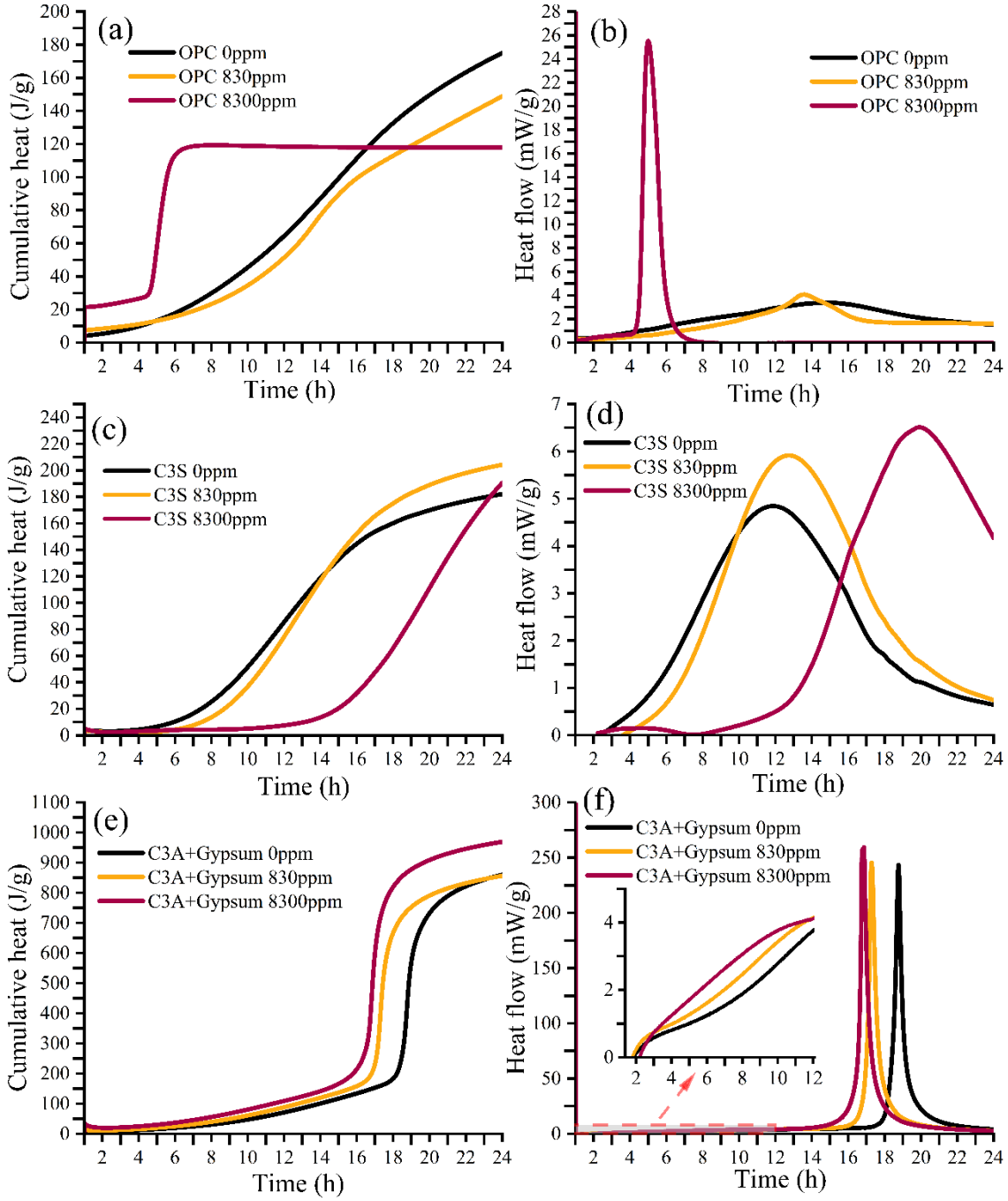

334

335 *3.3.Characterization of solids phase after adsorption*

336 *3.3.1. Results of powder XRD*

337 Given that OPC, pure C_3S, and CH are significantly related to the adsorption of TEA, the
338 phase transitions of the binders after adsorption were further investigated using XRD, as
339 shown in Fig. 4. Notably, the three types of solids exhibited different patterns with
340 changes in TEA dosage.

The most evident difference was observed in the intensities of the CH diffraction peaks. For OPC, the intensity of the (001) peak of CH located at approximately 18° gradually decreased with increasing TEA concentration. In particular, at 8300 ppm, almost no CH diffraction peak of CH is generated. Conversely, a broad diffraction peak was observed at approximately 10°, which likely corresponded to the solid solution of HC and monocarboaluminate [53] formed during C_3A hydration. This observation aligns well with the calorimetric results depicted in Fig. 3(b), where the sharp exothermic peak at approximately 5 h indicates rapid C_3A hydration [19]. For pure C_3S, although the intensity of the CH diffraction peaks decreased with increasing TEA concentration, the overall effect was negligible. The most interesting case was observed for pure CH, where the diffraction peak of CH remained unchanged, even when TEA was completely adsorbed onto CH. To address concerns regarding the influence of solvent changes on the crystal structure of CH, the XRD patterns of CH after adsorption using different hydration stoppage methods were examined, as shown in the supplementary data. The results were comparable, indicating that the results shown in Fig. 4 are reasonable to some extent.

It is hypothesized that physical adsorption is the primary adsorption method during the adsorption process because TEA does not alter the crystal structure of CH. It is also suggested that the structure of CH remains quite stable even in a high-dosage TEA environment. However, as suggested in previous studies, TEA may influence the formation and crystallization of CH by forming complexes with CH [11]. Wang et al. observed that TEA significantly influenced the crystallization process of CH using a coprecipitation method from an aqueous solution of $CaCl_2$ and NaOH [27]. With the incorporation of TEA, large amounts of micro- and non-crystalline CH were formed. Zhang et al. suggested that the complex of TEA and Ca^{2+} was the decisive factor controlling the crystallization of CH [26]. A significant difference in the amount of CH detected by TG and XRD was observed, which was attributed to the production of non-crystalline CH [18]. Notably, some alkanolamines including TEA and EDIPA could influence the morphology and crystal structure of CH during the co-precipitation process. However, it should be considered that seeding or co-precipitation processes may not accurately represent the real precipitation process of CH during OPC hydration due to the different solubility. One possible reason for the alteration in the CH growth process in the coprecipitation experiments was the use of $CaCl_2$ [27,54,55]. The high solubility of $CaCl_2$

allows for the easier introduction of additional admixtures into the precipitation process. Given that both the adsorption process in this study (where CH is already precipitated) and the coprecipitation process may not fully represent the real precipitation process of CH during OPC hydration, the primary reason for the nondetected CH in the OPC system during adsorption should be considered.

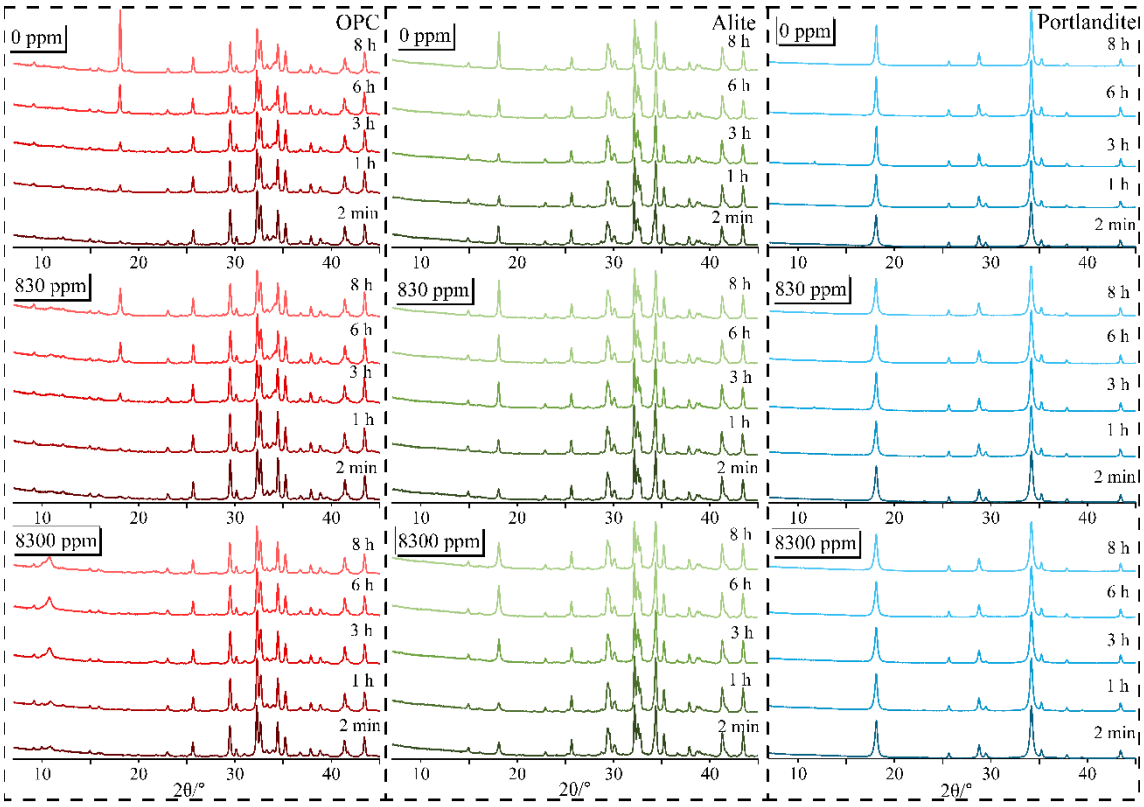

3.3.2. *Cross-sectional comparison of the quantified results*

To further confirm the presence of the CH, a mutual comparison was conducted. A comparison of the TG-DTG curves, which is acknowledged as a reliable method for determining the CH [56] content of OPC and C_3S at 1, 3, and 8 h after adsorption, is depicted in Fig. 5. A clear trend was observed, where more CH was generated with continued hydration. However, an exception was observed for the OPC with 8300 ppm TEA. Therefore, from 1 h to 8 h, while few CH molecules were generated at 1 h, the growth of CH appeared to be halted. These results well align with the XRD results.

Notably, observing phase transformations at the initial stage is quite challenging. A short hydration period may not be easily observed, and hydration stoppage may not be sufficient or timely. In some cases, the stoppage method can affect the crystal structure of

the hydration phase [57,58]. Therefore, in situ, XRD was employed to qualitatively observe the process of phase transformation during the first 104 h, which was selected based on the results of the heat flow of OPC at a TEA concentration of 8300 ppm. The results are shown in Fig. 6. Before 8 h, precipitation of the CH phase was not observed, which is consistent with the QXRD and TG results, as shown in Fig. 4 and 5, respectively. Subsequently, the formation of CH became pronounced until the end of the measurement, which verified the accuracy of the QXRD and TG results to some extent.

Therefore, the amount of CH in the OPC system measured by XRD and TG was corrected, as shown in Fig.7. Notably, the difference between the CH quantified by XRD and TG is inevitable [59], and because the quantification of the initial hydration is challenging, some errors may occur. However, the amount of CH measured by XRD was in reasonable agreement with the TG results. This is in contrast to previous observations, which suggested that TEA affects the crystal structure of CH [26,60], leading to a large discrepancy between the quantitative XRD and TGA results for CH.

Additionally, owing to the low hydration rate of C_2S in the initial stage, it was assumed that CH was entirely generated by the hydration of C_3S [34]. The relationship between the quantified C_3S consumption and CH generated by XRD is presented in Fig. 7, where the data fall near the dashed line of equality. Furthermore, thermodynamic modeling predicted the consumption of C_3S and precipitation of CH depending on the hydration time (Fig. 8). The relationship between the consumption of C_3S and precipitation of CH is fitted by a red line, as shown in the figure. Generally, the XRD data followed a fitted curve, except for the samples containing 8300 ppm TEA. This may be due to the inhibition of C_3S hydration in the high-dosage TEA environment, resulting in a small amount of CH being produced and higher errors in the quantitative analysis. Typically, phases below 0.5 wt% make quantitative analysis by XRD less representative [56]. The hydration of OPC is controlled by dissolution-precipitation mechanisms [61], whereas the addition of TEA can significantly alter the dissolution rate of alkali ions, further influencing the phase transformation. However, in this study, our main aim was to illustrate that the generated CH is in good agreement with the consumption of C_3S, which suggests that microcrystalline CH cannot be considered. In an actual OPC system, the adsorption of TEA on the CH surface does not inhibit CH growth in the initial stage. The low intensity of the (001) peak of CH is caused by the inhibition of C_3S hydration.

Additionally, in the experiment by Rodriguez-Navarro et al. [62], although the morphology of CH changed significantly, no significant changes in the XRD patterns were observed in the presence of additives. This indicated the complexity of the nucleation of CH in an environment with additives. The CH microcrystals observed in previous studies [26,27,63] could not be linked directly to the addition of TEA in this study. Other factors, such as the influence of the w/b ratio [8] and the interaction between the availability of gypsum and alumina[64], should be further considered.

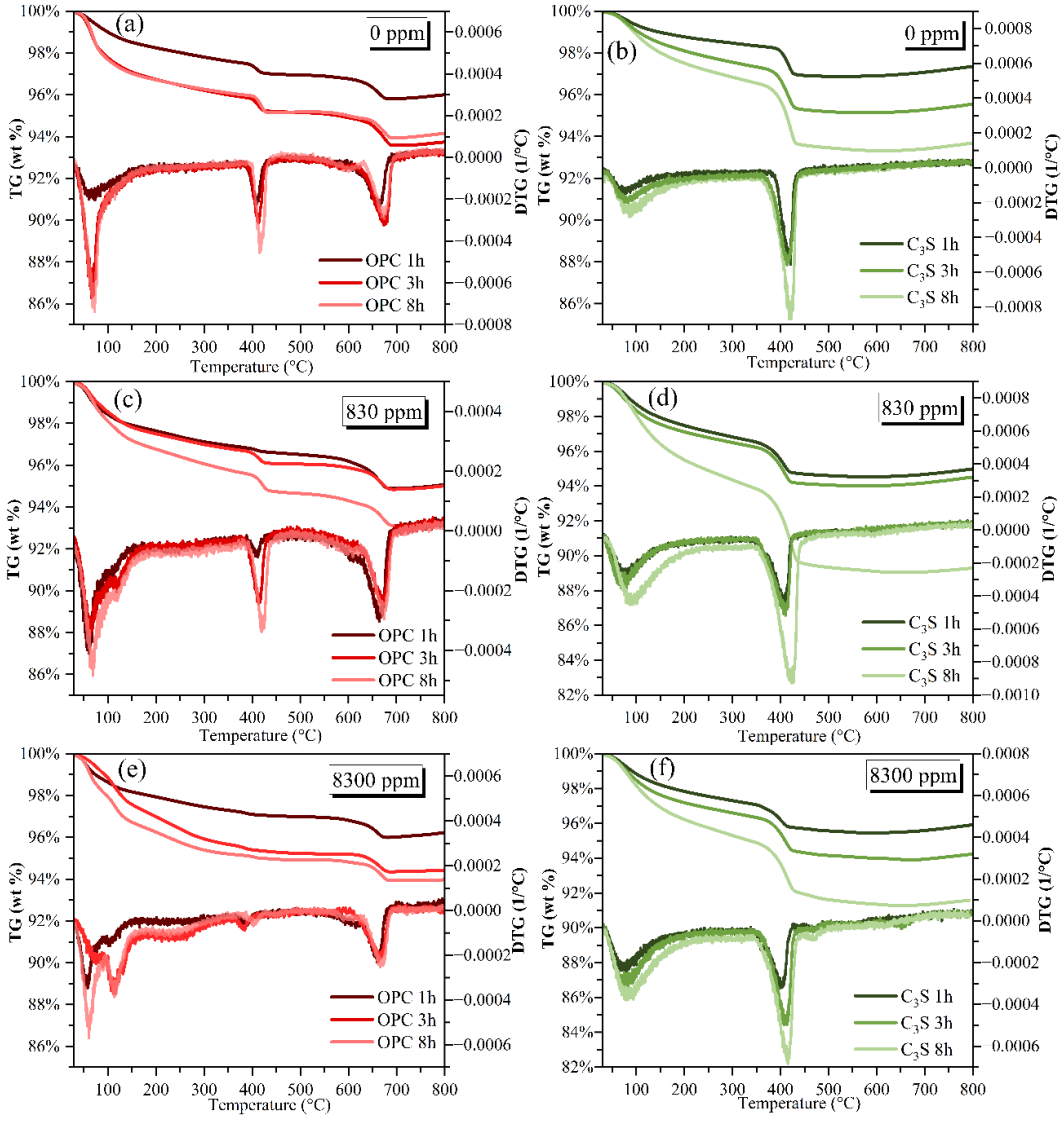

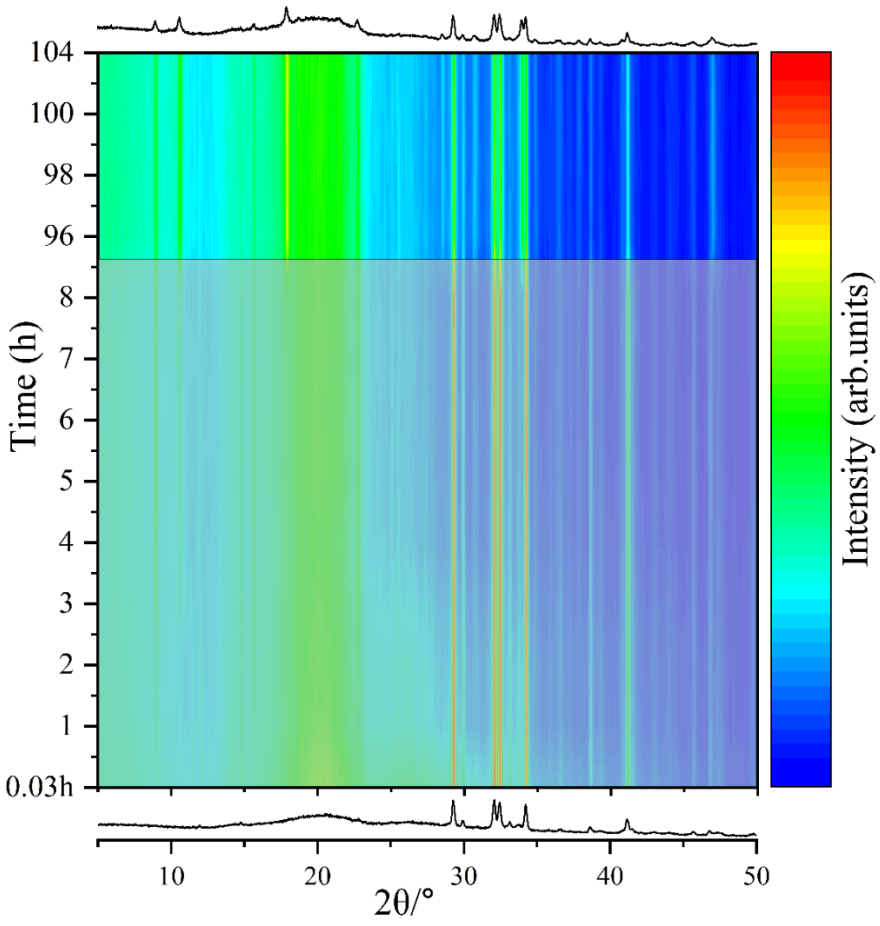

Fig. 6. Time-resolved XRD pattern of OPC in addition with 8300ppm TEA.

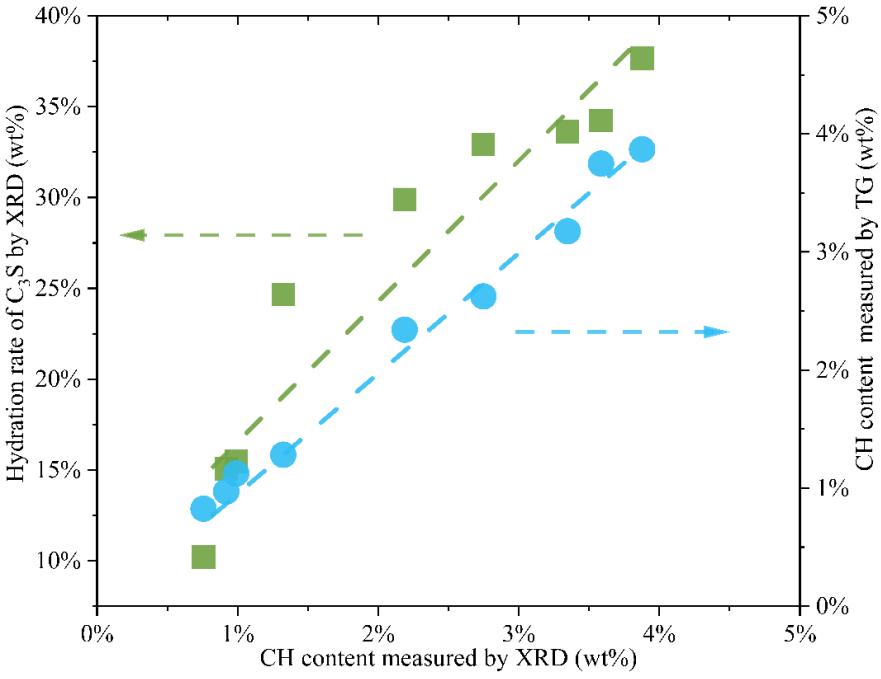

Fig. 7. Comparison of CH content measured by TG and XRD, and correlation between hydration degree of C_3S and CH content measured by XRD.

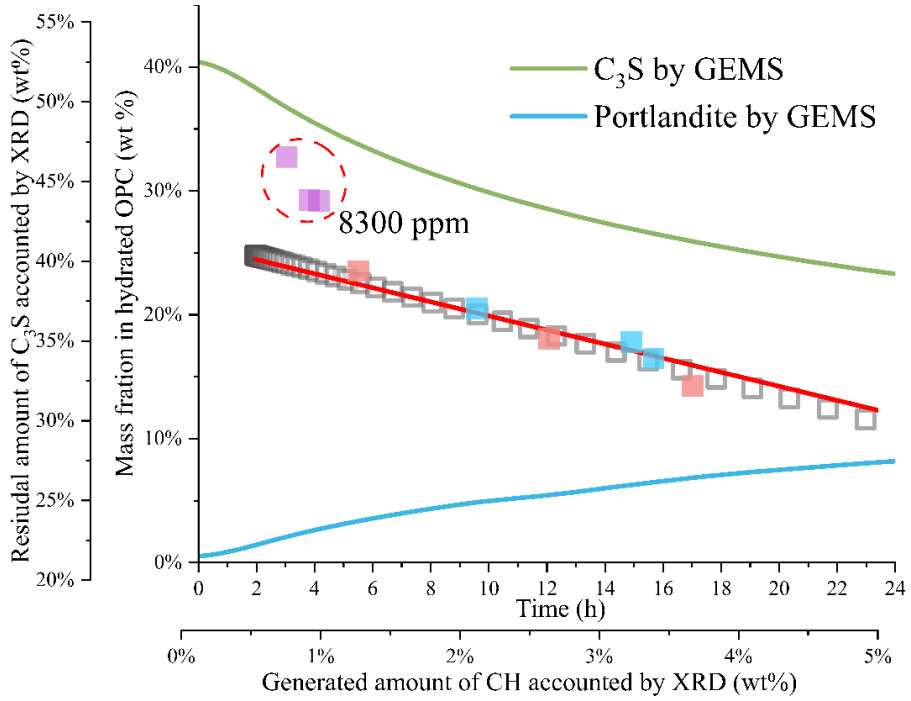

Fig. 8. Mass fraction of C_3S and CH in hydrated OPC by thermodynamic modeling, and correlation of mass fraction of C_3S and CH measured by XRD.

3.4.Adsorption energy of TEA on the surface of minerals by MD

Owing to the limitations of the experimental characterization, the underlying mechanism behind the varying adsorption behaviors of TEA on the surfaces of the four minerals in this study remains elusive. MD simulations were conducted to gain insight into this phenomenon. The initial configurations of the interaction model are depicted in Figure 9, and the details of the simulation box are listed in Table 2.

The mass density profile along the reference direction normal to the surface is shown in Fig. 10. The calculations highlighted a significant finding: TEA exhibited weak interaction with the mineral surfaces, regardless of mineral type. This interaction strength was quantified using adsorption energy, as detailed in [42,65].

$$\Delta E_{adp} = E_{mineral+TEA+water} - E_{mineral+water} - E_{TEA+water} + E_{water} \quad (3)$$

where ΔE_{adp} is the adsorption energy.

Data sampling and analysis methods for adsorption were conducted to align with Mishra's [65] approach. The thermodynamic data were sampled using block averages during the

452 final 1 ns of the equilibrium stage, comprising 10,000 snapshots. Each block comprised
453 50 snapshots, and the lowest average value was used for calculations. The adsorption
454 strength decreases in the following order: CH > GP > C_3A > C_3S (refer to Fig. 11). Notably,
455 except for CH, the adsorption was unfavorable. Even in the case of CH with an adsorption
456 energy of -6.83 kcal mol^{-1}, the strength of adsorption was relatively weak.
457 The obtained adsorption energy differed from that calculated in previous investigations
458 [6]. This is because a liquid station was used instead of a gas station in this study. These
459 simulations were performed to achieve a perfect plain surface cleavage. More favorable
460 adsorption energies can be obtained if defects and dislocations are included because these
461 undercoordinated sites are preferential adsorption/dissolution sites. The simulation results
462 were aligned well with the trends observed in the adsorption experiments. Regarding the
463 adsorption mechanism, Mishra et al. [6] attributed this to hydrogen bonding between the
464 alcoholic groups of TEA and acceptors from the minerals, along with calcium
465 complexation with surface ions from the minerals. The hydrogen bonding mechanism is
466 relatively straightforward to understand as a driving force. However, the proposed
467 mechanism does not fully explain why TEA tends to be complex with calcium ions rather
468 than with other ions present in the complex OPC system. OPC is a complex system
469 containing various alkali metal ions. Even within the single-phase system studied herein,
470 questions arise as to why TEA primarily forms a complex with calcium ions as the driving
471 force and not with other ions.

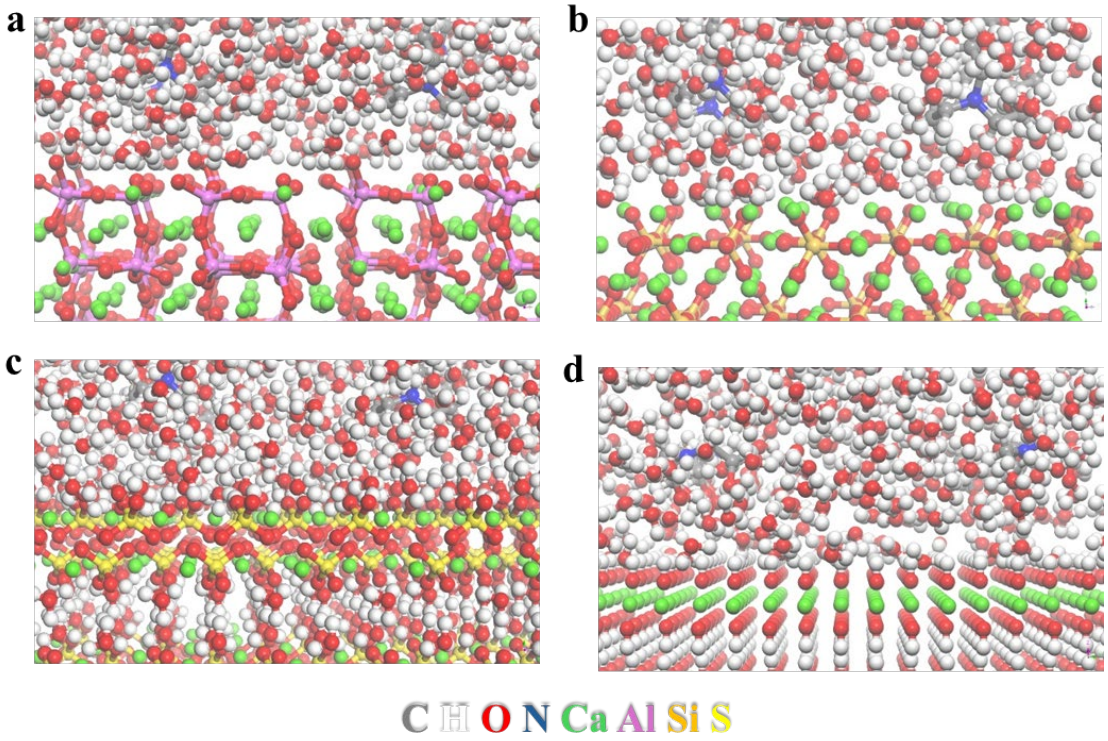

Fig. 9. Interaction surface model constructed with introduced TEA solution. (a) C_3A; (b) C_3S; (c) Gypsum; and (d) CH.

Table 2

Parameters of the interface model

Mineral	Miller indices	Size (Å)
C_3A	(010)	30*163*30
C_3S	(040)	24*217*25
Gypsum	(010)	34*133*34
Portlandite	(001)	31*32*140

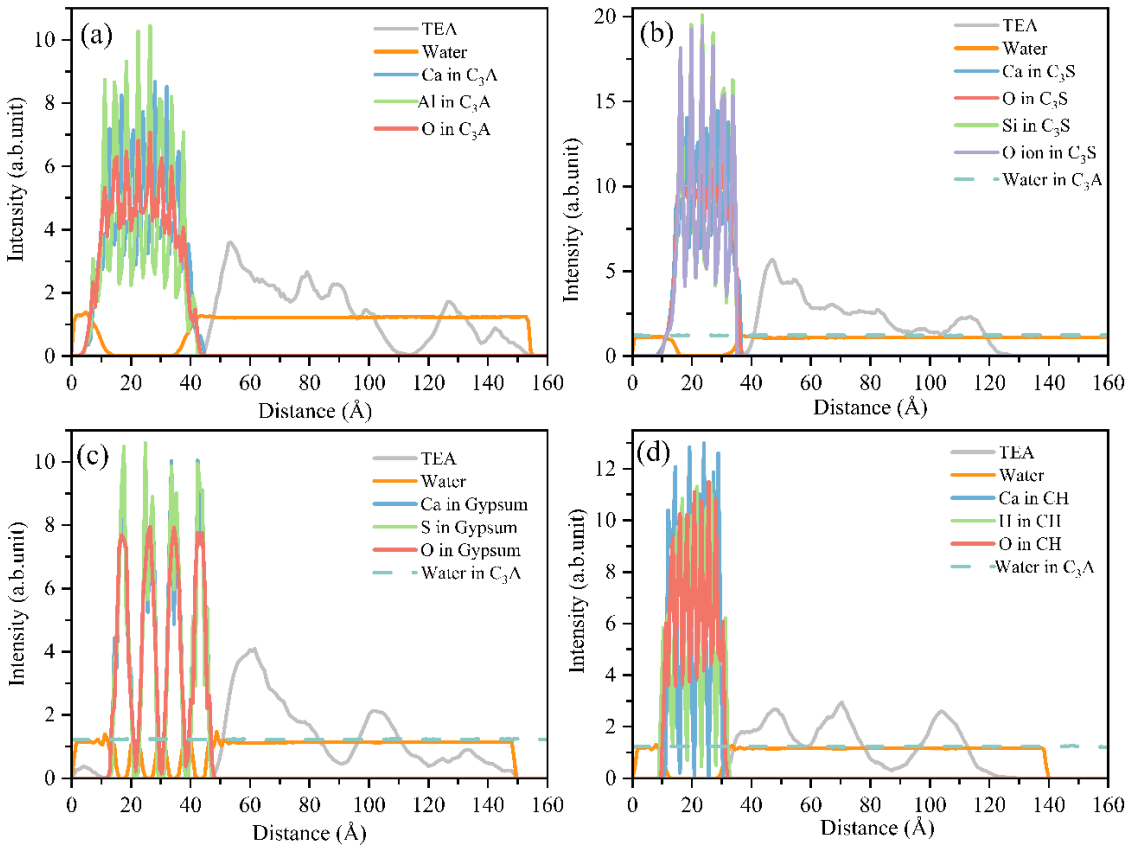

Fig. 10. Density profile along the reference direction of TEA solution with (a) C_3A; (b) C_3S; (c) Gypsum; and (d) CH.

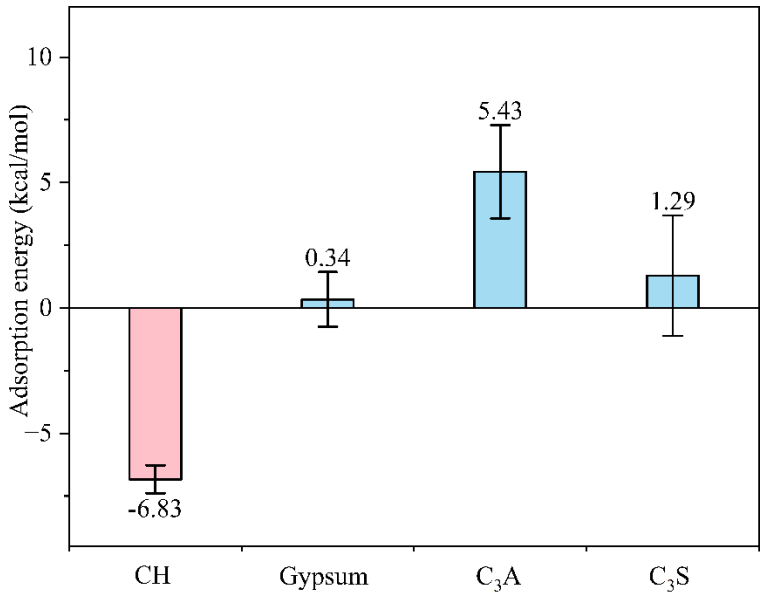

Fig. 11. Adsorption energy of TEA on the surface of minerals.

3.5.Complexation energy of TEA-metal complexes

To better understand the complexation properties, static and dynamic electronic structure calculations of the TEA complex with common alkali metal ions were performed using DFT. Notably, the complexation between Fe and TEA was not calculated. While C_4AF can dissolve rapidly in the first 15 min at high TEA concentrations, as reported by Lu et al. [19], our measurements in the OPC system revealed only insignificant changes in the TEA concentration. Additionally, it is crucial to consider that Fe, as a transition metal, is not ideally suited for the functional group and basis set selected for the main group elements in DFT calculations. As reported by Naiini et al. [66], most metals from Groups 1 and 2 are unable to form an Atrane-like structure (i.e., the ratio of ligand to receptor cannot be 1:1) owing to their low oxidation states. The structure of two ligating TEA molecules complexed to a single ion was also studied. Frontier orbitals of the complexes and their energy gaps are depicted in Fig. 12. When the ligand-to-metal ratio was 1:1, the HOMO of TEA was uniformly dispersed throughout the whole structure, excluding hydrogen atoms, while the LUMO mainly localized around oxygen atoms. This aligns with the results shown in [67]. After complexing, the HOMO of the metal-TEA complex remained uniformly dispersed, whereas the LUMO localized predominantly at the metal sites. The 2TEA-Ca complex exhibited a similar behavior. For complexes involving Na, Mg, and Al, the HOMO was dispersed through only one TEA ligand. This suggests that the other TEA ligands contributed less to the overall properties of the complexes because of the lack of a significant electron cloud. The HOMO–LUMO transition during excitation can redistribute electron density from metal moieties to TEA, thereby resulting in effective intramolecular charge transfer in the complex. Additionally, the interaction of Ca and Na ions with TEA reduces the HOMO-LUMO energy gap, resulting in increased chemical reactivity.

The free energy of complexation in solution was calculated using the method proposed in a previous study [43,68]. A schematic of this process is shown in Fig. 13. The first layer of solvent coordination is the most important factor for calculating the hydration energies [68]. Therefore, for simplicity, only the first coordination shell with six water molecules [43] is considered. The free energy changes of complexation in solution ($\Delta_{comp}G(aq)$ are calculated as follows:

$$\Delta_{comp}G(aq) = \Delta_{comp}G(gas) + \Delta\Delta_{sol}G \quad (4)$$

$$\Delta\Delta_{sol}G = \Delta_{sol}GMTEA + 6 \times \Delta_{sol}G(H_2O) - \Delta_{sol}GTEA - \Delta_{sol}GM(H_2O)_6 \quad (5)$$

where $\Delta_{comp}G(gas)$ is free energy changes of complexation in gas, and $\Delta\Delta_{sol}G$ is the contribution of the solvation effect to the complexation reaction.

The calculated complexation energies are shown in Fig. 14. The stability order for the complexes with different metal ions was $Ca^{2+} > Na^{+} > Mg^{2+}$, whereas the positive value of the complexation free energy in the case of Al indicated unfavorable thermodynamics of the complex formation process. This result could be well explained by MD, where Ca complexation can be one of the driving forces for adsorption rather than the other elements.

Additionally, a favorable reaction for the complexation of an ion with two TEA ligands has been demonstrated. The complexation energy for an ion with two TEA ligands was significantly lower than that with one TEA ligand. Specifically, the free energy change for the Ca-2TEA complex was nearly 60 kcal/mol lower than that of the Ca-TEA complex. This indicates the higher stability of the 1:2 Ca-TEA complex in contrast to the 1:1 complex.

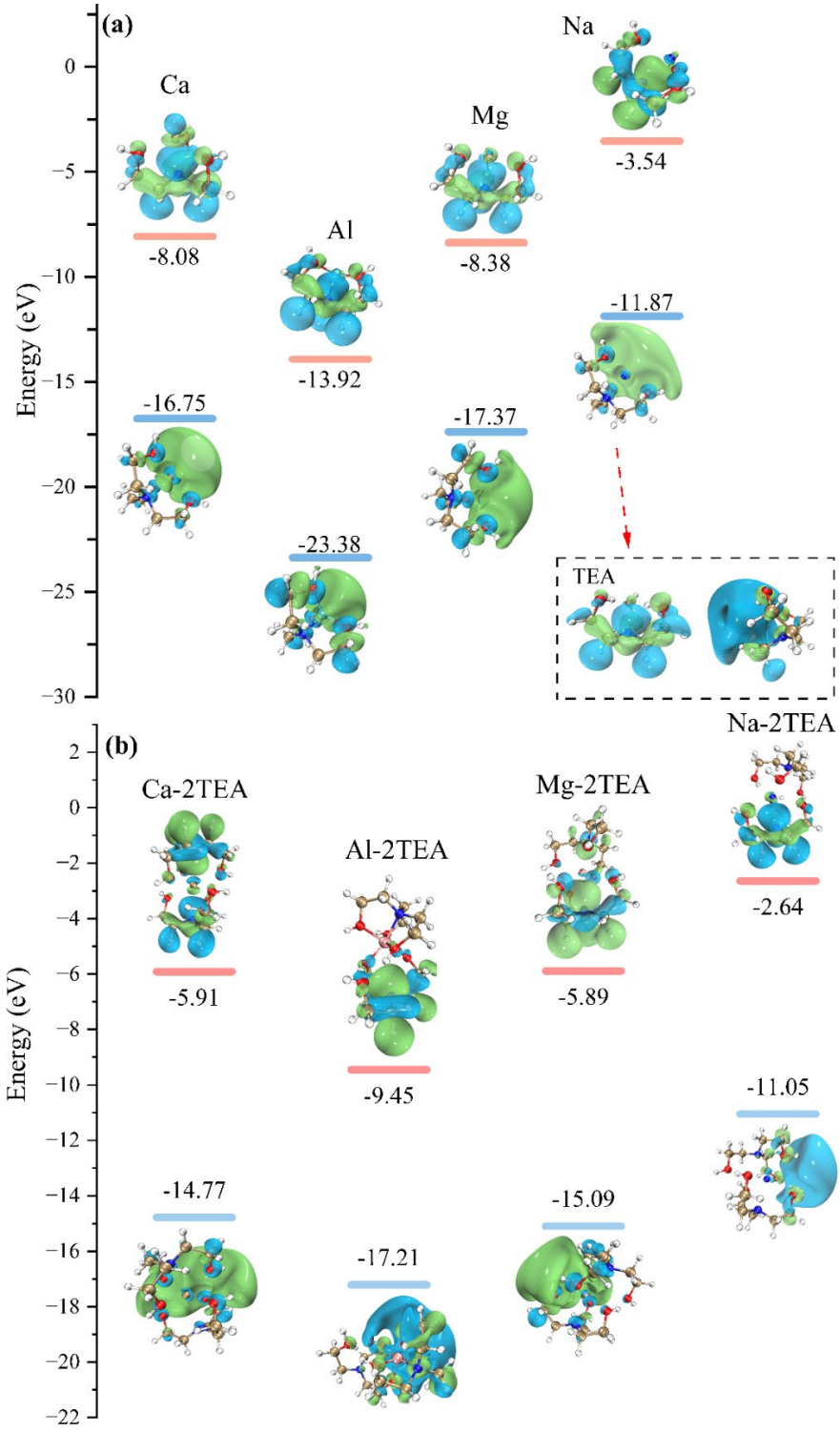

Fig. 12. Comparison of the highest molecular orbital (HOMO)-lowest unoccupied molecular orbital (LUMO) energy levels for common elements during the initial dissolution of OPC at the M06-2X/def2-TZVPP level of theory. Note: Only the structure optimized in the gas environment is shown.

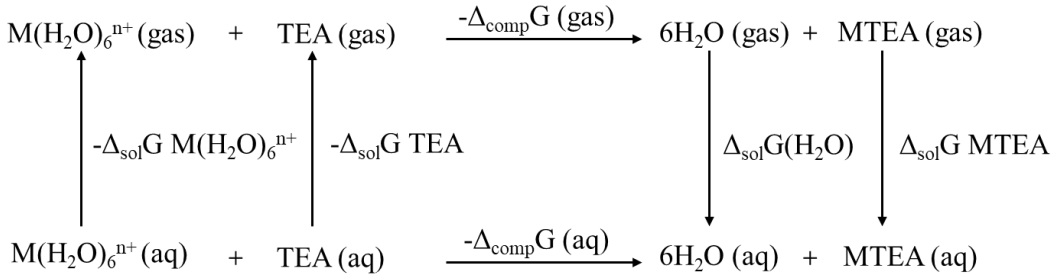

Fig. 13. Thermodynamic cycle used to determine the complexation energy in solution.

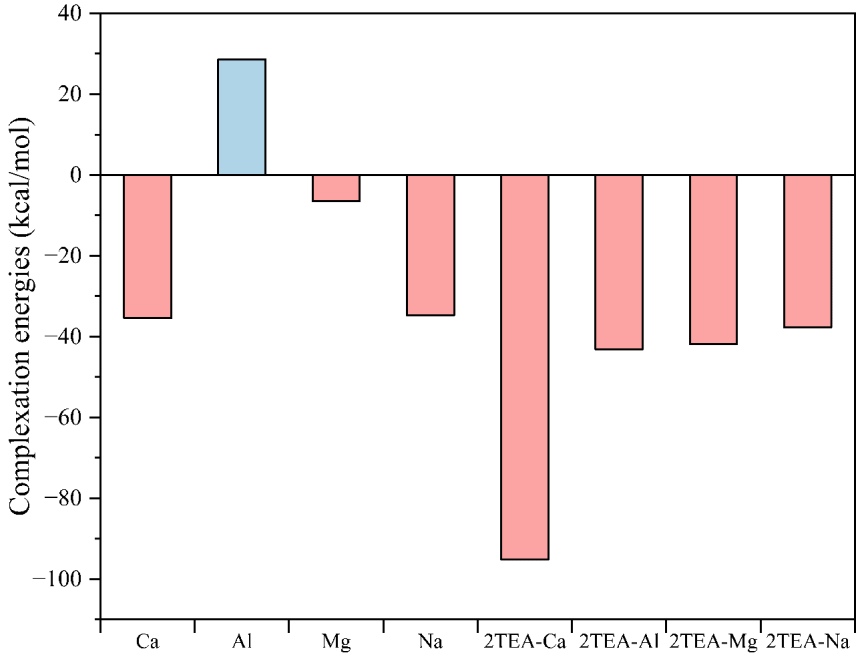

Fig. 14. Complex energy between TEA and metal ions in water.

3.6.Binding capacity of CH

It is well known that during the hydration of C_3S, both CH and C-S-H, which constitute the majority of the hydration phases, are generated. Therefore, clarifying the contribution of C-S-H to the adsorption process was crucial. For simplicity, the potential of C-S-H to act as an acceptor was determined by the adsorption capacity of CH, which was determined from the isotherm adsorption curve. According to Fig. 2, it was assumed that 1 d was sufficient for full adsorption. Therefore, pure CH mixed with different dosages of TEA (830, 1660, 3320, 4980, 6640, and 8300 ppm in theoretical units) was shaken for 1 d, following identical post-processing steps as described in Section 2.2.2. The adsorption isotherms are shown in Fig. 15. Fig. 15 shows that the adsorbed amount of TEA increased sharply at low dosages and finally reached a plateau. Errors are inevitable

because of the high dosages tested in this study. This trend shows a good agreement, as shown in Fig. 2, and explains the assumptions proposed in Section 3.1.

While the TEA concentration in the pore solution can be measured, the free water decreases during this process because of the continual hydration of the OPC. Therefore, it is difficult to accurately quantify the amount of TEA adsorbed after hydration. The amount of free water after adsorption (m_{sa} was estimated from the LOI, and the adsorption amount was calculated using the following formula:

$$m_{ad} = C_{i,ppm} m_{si} - C_{a,ppm} m_{sa} * (1 - LOI) \quad (6)$$

where m_{ad} (mg) is the amount of adsorbed TEA, C_i, ppm is the concentration of TEA before adsorption, m_{wi} is the amount of TEA solution before adsorption, and $C_{a,ppm}$ is the concentration of TEA after adsorption.

The adsorption limit of CH is estimated by the equation:

$$AL_{CH} = BC_{CHad} * m_{raw} * \omega_{CH,t} \quad (7)$$

where AL_{CH} is the adsorption limit of CH (mg), BC_{CH} is the binding capacity of CH in the pure CH system (mg/g), m_{raw} is the amount of raw materials used in the adsorption experiment, and ω_{CH} is the mass fraction of CH generated in OPC and C_3S at a specific age t measured by TG.

Considering the low adsorption before 3 h, the specific ages at 3 and 8 h were selected for comparison. The amounts of TEA adsorbed, and the adsorption limits of CH are compared in Table 3. Owing to the low degree of hydration of OPC with the addition of 8300 ppm TEA, a comparison was not performed in this system. As shown in Table 3, before 3 h, the adsorbed TEA in the C_3S and OPC systems did not exceed the adsorption limit of CH. This suggests that before or during the initial main hydration of C_3S (Fig. 3), CH primarily acts as the acceptor of TEA. However, by 8 h, the amount of TEA absorbed in each system had exceeded the upper limit of CH absorption. This indicates that as the C_3S reaction progressed, resulting in the production of large amounts of C-S-H, the primary acceptor role shifted from CH to C-S-H, although CH continued to play a role as an acceptor of TEA.

However, as indicated in Sections 3.4 and 3.5, the complex formation mechanism is mainly driven by hydrogen bonds and Ca complexation. Considering that both CH and

C-S-H provide the necessary factors for complex formation, it is challenging to determine whether competitive adsorption occurs between CH and C-S-H. In this study, we simplified the conditions and determined whether C-S-H can act as an acceptor based on the adsorption limit of CH. Moreover, owing to the uncertainties caused by the high dosage of TEA, further investigation into the adsorption ability of C-S-H and potential competitive interactions is imperative for future research.

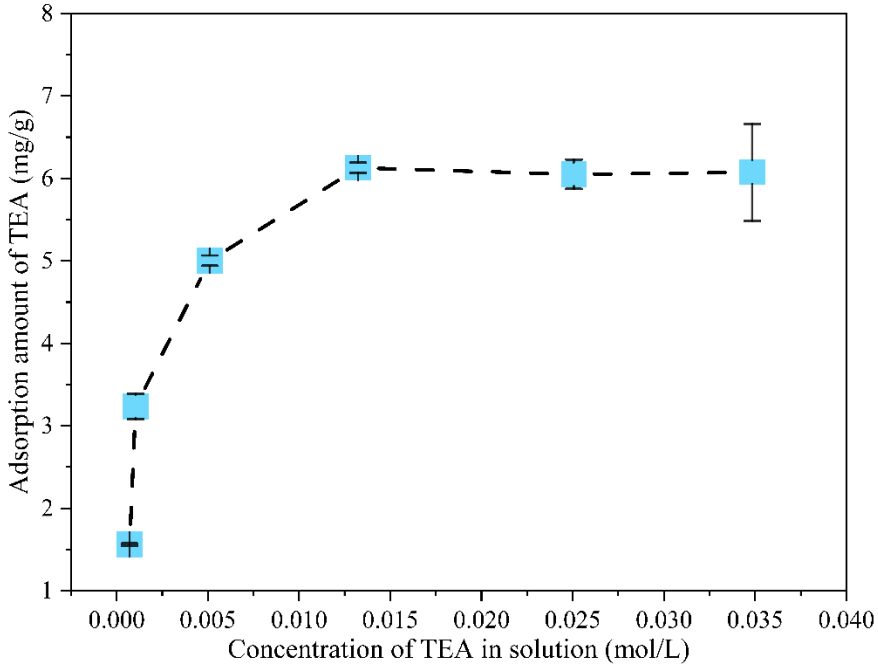

Fig. 15. Adsorption isotherms of TEA on the surface of CH.

Table 3

Comparison of the adsorption limit of CH and the adsorbed amount of TEA in OPC and C_3S (mg).

Dosage	Period	AL_{CH} in OPC	m_{ad} in OPC	AL_{CH} in C_3S	m_{ad} in C_3S
830 ppm	3h	0.23	0.21	0.77	0.55
	8h	0.35	2.38	0.35	2.31
8300 ppm	3h	/	/	3.81	1.07
	8h	/	/	3.36	14.18

4. Conclusions

The adsorption of TEA at concentrations of 830 and 8300ppm in OPC, pure C_3S, gypsum, gypsum+C_3A, and pure CH was thoroughly investigated using various techniques including TOC, XRD, TG, isothermal calorimetry, thermodynamic modeling, MD, and DFT. The following observations were made:

Throughout the adsorption process, it was found that the adsorption of TEA was closely related to the hydration of C_3S. It was observed that TEA did not adsorb directly onto C_3S, but rather onto the hydration products of C_3S, that is, CH and C-S-H. In the early stage of the accelerated hydration of OPC, TEA was mainly adsorbed on CH. The MD calculations supported this observation, thereby indicating that among C_3S, C_3A, gypsum, and CH, CH exhibited the lowest adsorption energy. Furthermore, calculations of the amount of TEA adsorbed and the adsorption capacity of CH indicated that at a later stage of the accelerated hydration period, the adsorption significantly exceeded the upper limit of the adsorption capacity of CH. As the hydration of C_3S progresses, the role of the TEA receptor may shift to that of C-S-H.

As suggested by many researchers, TEA inhibits CH growth. Our results reveal that while TEA can adsorb on the surface of CH, in the initial stage of OPC with a high dosage of TEA, it promotes the hydration of C_3A. However, the hydration of C_3S is strongly inhibited, which further impedes the crystal growth of CH. This is indicated by the persistently high TEA concentration in the solution.

According to the XRD results, the crystal structure of CH remained unchanged during the adsorption process in the pure CH mixed with the TEA system. This suggests that TEA was physically adsorbed on the surface of CH. The MD results further confirmed this, showing that while the adsorption energy was negative, the value was relatively high, and the density profile of TEA was higher in the solution than near the surface. This indicates that TEA adsorption was weak.

In elucidating the adsorption mechanism, it was found that TEA adsorption is primarily driven by hydrogen bonding and Ca complexation. Density functional theory (DFT) calculations were used to compute the complexation energies between TEA and various ions (Ca^{2+}, Mg^{2+}, Na^{+}, and Al^{3+}) at a ligand-to-metal ratio of 1:1. Among these, the TEA-Ca^{2+} complex exhibited the lowest complexation energy. Additionally, the complex formed between TEA and Ca^{2+} in a 2:1 ratio was found to be more stable.

Acknowledgement

This study was supported by JSPS KAKENHI [Grant Number: 21K04349]. H.M acknowledges the support by the “Departamento de Educación, Política Lingüística y Cultura del Gobierno Vasco” (Grant No. IT1458-22),

CRediT authorship contribution statement

Qi Zhai: Methodology, investigation, writing–original draft, and conceptualization. Kiyofumi Kurumisawa conceptualized, reviewed, edited, and supervised the study. Juhyuk Moon: Review and editing. In-Hee Hwang: Methodology, review, and editing. Hegoi Manzano: Methodology, review, and editing.

Compliance with ethics guidelines

Qi Zhai, Kiyofumi Kurumisawa, Juhyuk Moon, Hegoi Manzano and In-Hee Hwang declare no competing financial interests or personal relationships that may have influenced the work reported in this study.

References

[1] M. Katsioti, P.E. Tsakiridis, P. Giannatos, Z. Tsibouki, J. Marinos, Characterization of various cement grinding aids and their impact on grindability and cement performance, Constr. Build. Mater. 23 (2009). https://doi.org/10.1016/j.conbuildmat.2008.09.003.

[2] X. Liao, H. Huang, F. He, C. Yang, Microstructural characterization of cement in the presence of alkanolamines, Mater. Today Commun. 27 (2021) 102386. https://doi.org/10.1016/j.mtcomm.2021.102386.

[3] V. Chipakwe, P. Semsari, T. Karlkvist, J. Rosenkranz, S.C. Chelgani, A critical review on the mechanisms of chemical additives used in grinding and their effects on the downstream processes, Mater. Res. Technol. 9 (2020) 8148–8162. https://doi.org/10.1016/j.jmrt.2020.05.080.

[4] W. Li, S. Ma, Y. Hu, X. Shen, The mechanochemical process and properties of Portland cement with the addition of new alkanolamines, Powder Technol. 286 (2015) 750–756. https://doi.org/10.1016/j.powtec.2015.09.024.

[5] M. Jachiet, N. Azéma, G. Le Saoût, E. Garcia-Diaz, V. Kocaba, Influence of triethanolamine on cement pastes at early age of hydration, Adv. Cem. Res. 30 (2018) 159–171. https://doi.org/10.1680/jadcr.17.00041.

[6] R.K. Mishra, R.J. Flatt, H. Heinz, Force field for tricalcium silicate and insight into nanoscale properties: Cleavage, initial hydration, and adsorption of organic

molecules, J. Phys. Chem. C 117 (2013) 10417–10432. https://doi.org/10.1021/jp312815g.

[7] T. Lee, J. Lee, H. Choi, D.E. Lee, The effects of fineness and TEA-based chemical admixture on early strength development of concrete in construction site applications, Materials 13 (2020). https://doi.org/10.3390/MA13092027.

[8] X. Wang, M. Wei, K. Liu, K. Cui, Y. Yang, Z. Tian, Particle size of calcium hydroxide prepared by wet digestion: Influencing factors and mechanism, Cryst. Res. Technol. (2024). https://doi.org/10.1002/crat.202300335.

[9] J. Jiang, B. Liu, J. Shi, O. Gencel, X. An, J. Gao, Synergistic effect of glycine and triethanolamine on mechanical properties and permeability of cement mortar, J. Build. Eng. 51 (2022) 104283. https://doi.org/10.1016/j.jobe.2022.104283.

[10] Z. Lu, X. Peng, T. Dorn, T. Hirsch, D. Stephan, Early performances of cement paste in the presence of triethanolamine: Rheology, setting and microstructural development, J. Appl. Polym. Sci. 138 (2021). https://doi.org/10.1002/app.50753.

[11] V.S. Ramachandran, Influence of triethanolamine on the hydration characteristics of tricalcium silicate, J. Appl. Chem. Biotechnol. 22 (2007) 1125–1138. https://doi.org/10.1002/jctb.5020221102.

[12] Z. Xu, W. Li, J. Sun, Y. Hu, K. Xu, S. Ma, X. Shen, Hydration of Portland cement with alkanolamines by thermal analysis, J. Therm. Anal. Calorim. 131 (2018) 37–47. https://doi.org/10.1007/s10973-017-6271-y.

[13] V.H. Dodson, Concrete Admixtures, Springer US, 1990. https://doi.org/10.1007/978-1-4757-4843-7.

[14] Q. Zhai, K. Kurumisawa, J. Moon, I.H. Hwang, Advances in understanding the effect of alkanolamine in cement-based materials, J. Clean. Prod. 452 (2024). https://doi.org/10.1016/j.jclepro.2024.142167.

[15] H. Xie, X. Liu, Y. Zheng, B. Chi, J. Guo, X. Dai, Z. Zhang, M. Sun, L. Duan, Z. Wang, S. Cui, Effect of complexation of alkanolamine in accelerators on the initial stage of cement hydration, Constr. Build. Mater. 393 (2023) 132105. https://doi.org/10.1016/j.conbuildmat.2023.132105.

[16] Y.L. Yaphary, Z. Yu, R.H.W. Lam, D. Lau, Effect of triethanolamine on cement hydration toward initial setting time, Constr. Build. Mater. 141 (2017) 94–103. https://doi.org/10.1016/j.conbuildmat.2017.02.072.

[17] T. Hirsch, Z. Lu, D. Stephan, Impact of triethanolamine on the sulfate balance of Portland cements with mixed sulfate carriers, J. Am. Ceram. Soc. 104 (2021) 4829–4842. https://doi.org/10.1111/jace.17913.

[18] V.S. Ramachandran, Hydration Of Cement-Role Of Triethanolamine, Pergamon Press, Inc, 1976.

[19] Z. Lu, X. Kong, D. Jansen, C. Zhang, J. Wang, X. Pang, J. Yin, Towards a further understanding of cement hydration in the presence of triethanolamine, Cem. Concr. Res. 132 (2020) 106041. https://doi.org/10.1016/j.cemconres.2020.106041.

[20] T. Hirsch, Z. Lu, D. Stephan, Effect of different sulphate carriers on Portland cement hydration in the presence of triethanolamine, Constr. Build. Mater. 294 (2021). https://doi.org/10.1016/j.conbuildmat.2021.123528.

[21] J. Han, K. Wang, J. Shi, Y. Wang, Mechanism of triethanolamine on Portland cement hydration process and microstructure characteristics, Constr. Build. Mater. 93 (2015) 457–462. https://doi.org/10.1016/j.conbuildmat.2015.06.018.

[22] X.-M. Kong, Z.-B. Lu, H. Liu, D.-M. Wang, Influence of triethanolamine on the hydration and the strength development of cementitious systems, Mag. Concr. Res. 65 (2013) 1101–1109. https://doi.org/10.1680/macr.13.00015.

[23] Y. Zhang, L. Gao, X. Cai, Q. Li, X. Kong, Influences of triethanolamine on the performance of cement pastes used in slab track, Constr. Build. Mater. 238 (2020). https://doi.org/10.1016/j.conbuildmat.2019.117670.

[24] J.P. Perez, A. Nonat, S. Garrault, S. Pourchet, M. Mosquet, Influence of triisopropanolamine on the physico-chemical and mechanical properties of pure cement pastes and mortars, in: Annales de Chimie: Science Des Materiaux, 2003.

[25] R.K. Mishra, L. Fernández-Carrasco, R.J. Flatt, H. Heinz, A force field for tricalcium aluminate to characterize surface properties, initial hydration, and organically modified interfaces in atomic resolution, Dalton Trans. 43 (2014) 10602–10616. https://doi.org/10.1039/C4DT00438H.

[26] Z. Yan-Rong, K. Xiang-Ming, L. Zi-Chen, L. Zhen-Bao, Z. Qing, D. Bi-Qin, X. Feng, Influence of triethanolamine on the hydration product of portlandite in cement paste and the mechanism, Cem. Concr. Res. 87 (2016) 64–76. https://doi.org/10.1016/j.cemconres.2016.05.009.

[27] J. Wang, X. Kong, J. Yin, S. Li, Impacts of two alkanolamines on crystallization and morphology of calcium hydroxide, Cem. Concr. Res. 138 (2020) 106250. https://doi.org/10.1016/j.cemconres.2020.106250.

[28] S.A. Weckwerth, R.L. Temme, R.J. Flatt, Experimental method and thermodynamic model for competitive adsorption between polycarboxylate comb copolymers, Cem. Concr. Res. 151 (2022). https://doi.org/10.1016/j.cemconres.2021.106523.

[29] N. Doebelin, R. Kleeberg, Profex: A graphical user interface for the Rietveld refinement program BGMN, J. Appl. Crystallogr. 48 (2015). https://doi.org/10.1107/S1600576715014685.

[30] Q. Zhai, K. Kurumisawa, Effects of cation in sulfate chloride and nitrite on Ca(OH)2 activated ground granulated blast-furnace slag, Cem. Concr. Compos. 133 (2022). https://doi.org/10.1016/j.cemconcomp.2022.104648.

[31] D.C. Chu, J. Kleib, M. Amar, M. Benzerzour, N.E. Abriak, Determination of the degree of hydration of Portland cement using three different approaches: Scanning electron microscopy (SEM-BSE) and Thermogravimetric analysis (TGA), Case Stud. Constr. Mater. 15 (2021). https://doi.org/10.1016/j.cscm.2021.e00754.

[32] D.A. Kulik, T. Wagner, S. V. Dmytrieva, G. Kosakowski, F.F. Hingerl, K. V. Chudnenko, U.R. Berner, GEM-Selektor geochemical modeling package: Revised algorithm and GEMS3K numerical kernel for coupled simulation codes, Comput. Geosci. 17 (2013). https://doi.org/10.1007/s10596-012-9310-6.

[33] B. Lothenbach, D.A. Kulik, T. Matschei, M. Balonis, L. Baquerizo, B. Dilnesa, G.D. Miron, R.J. Myers, Cemdata18: A chemical thermodynamic database for hydrated Portland cements and alkali-activated materials, Cem. Concr. Res. 115 (2019) 472–506. https://doi.org/10.1016/j.cemconres.2018.04.018.

[34] B. Lothenbach, F. Winnefeld, Thermodynamic modelling of the hydration of Portland cement, Cem. Concr. Res. 36 (2006) 209–226. https://doi.org/10.1016/j.cemconres.2005.03.001.

[35] H. Heinz, T.J. Lin, R. Kishore Mishra, F.S. Emami, Thermodynamically consistent force fields for the assembly of inorganic, organic, and biological nanostructures: The INTERFACE force field, Langmuir 29 (2013). https://doi.org/10.1021/la3038846.

[36] R.K. Mishra, K. Kanhaiya, J.J. Winetrout, R.J. Flatt, H. Heinz, Force field for calcium sulfate minerals to predict structural, hydration, and interfacial properties, Cem. Concr. Res. 139 (2021). https://doi.org/10.1016/j.cemconres.2020.106262.

[37] J. da S. Andrade Neto, A.G. De la Torre, A.P. Kirchheim, Effects of sulfates on the hydration of Portland cement – A review, Constr. Build. Mater. 279 (2021) 122428. https://doi.org/10.1016/j.conbuildmat.2021.122428.

[38] J. Claverie, F. Bernard, J.M.M. Cordeiro, S. Kamali-Bernard, Water's behaviour on Ca-rich tricalcium silicate surfaces for various degrees of hydration: A molecular dynamics investigation, J. Phys. Chem. Solids 132 (2019). https://doi.org/10.1016/j.jpcs.2019.03.020.

[39] C. Qi, H. Manzano, D. Spagnoli, Q. Chen, A. Fourie, Initial hydration process of calcium silicates in Portland cement: A comprehensive comparison from molecular

dynamics simulations, Cem. Concr. Res. 149 (2021). https://doi.org/10.1016/j.cemconres.2021.106576.

[40] K. Kanhaiya, M. Nathanson, P.J. in ’t Veld, C. Zhu, I. Nikiforov, E.B. Tadmor, Y.K. Choi, W. Im, R.K. Mishra, H. Heinz, Accurate force fields for atomistic simulations of oxides, hydroxides, and organic hybrid materials up to the micrometer scale, J. Chem. Theory Comput. 19 (2023) 8293–8322. https://doi.org/10.1021/acs.jctc.3c00750.

[41] A.P. Thompson, H.M. Aktulga, R. Berger, D.S. Bolintineanu, W.M. Brown, P.S. Crozier, P.J. in ’t Veld, A. Kohlmeyer, S.G. Moore, T.D. Nguyen, R. Shan, M.J. Stevens, J. Tranchida, C. Trott, S.J. Plimpton, LAMMPS - a flexible simulation tool for particle-based materials modeling at the atomic, meso, and continuum scales, Comput. Phys. Commun. 271 (2022). https://doi.org/10.1016/j.cpc.2021.108171.

[42] H. Heinz, Computational screening of biomolecular adsorption and self-assembly on nanoscale surfaces, J. Comput. Chem. 31 (2010). https://doi.org/10.1002/jcc.21421.

[43] L. Chen, T. Liu, C. Ma, Metal complexation and biodegradation of EDTA and *S* , *S* -EDDS: A density functional theory study, J. Phys. Chem. A 114 (2010) 443–454. https://doi.org/10.1021/jp904296m.

[44] N. Rahbani, P. de Silva, E. Baudrin, Density functional theory-based protocol to calculate the redox potentials of first-row transition metal complexes for aqueous redox targeting flow batteries, ChemSusChem. 16 (2023). https://doi.org/10.1002/cssc.202300482.

[45] Z. Chen, Y. Li, Z. He, Y. Xu, W. Yu, Theoretical investigations on charge transport properties of tetrabenzo[a,d,j,m]coronene derivatives using different density functional theory functionals (B3LYP, M06-2X, and wB97XD), J. Chem. Res. 48 (2019). https://doi.org/10.1177/1747519819861626.

[46] T. Lu, Q. Chen, Shermo: A general code for calculating molecular thermochemistry properties, Comput. Theor. Chem. 1200 (2021). https://doi.org/10.1016/j.comptc.2021.113249.

[47] I.M. Alecu, J. Zheng, Y. Zhao, D.G. Truhlar, Computational thermochemistry: Scale factor databases and scale factors for vibrational frequencies obtained from electronic model chemistries, J. Chem. Theory Comput. 6 (2010). https://doi.org/10.1021/ct100326h.

[48] T. Lu, F. Chen, Multiwfn: A multifunctional wavefunction analyzer, J. Comput. Chem. 33 (2012). https://doi.org/10.1002/jcc.22885.

[49] W. Humphrey, A. Dalke, K. Schulten, VMD: Visual molecular dynamics, J. Mol. Graph. 14 (1996). https://doi.org/10.1016/0263-7855(96)00018-5.

[50] T.N. O, É. DE Polytechnique fédérale lausanne, Hydration of C 3 A with calcium sulfate alone and in the presence of calcium silicate Alexandra QUENNOz, 2011.

[51] P. Juilland, A. Kumar, E. Gallucci, R.J. Flatt, K.L. Scrivener, Effect of mixing on the early hydration of alite and OPC systems, Cem. Concr. Res. 42 (2012). https://doi.org/10.1016/j.cemconres.2011.06.011.

[52] E. Gartner, D. Myers, Influence of Tertiary Alkanolamines on Portland Cement Hydration, J. Am. Ceram. Soc. 76 (1993) 1521–1530. https://doi.org/10.1111/j.1151-2916.1993.tb03934.x.

[53] Q. Zhai, K. Kurumisawa, J. Moon, A comparative study of alkanolamines and inorganic additives on the microstructure development of blast furnace slag blended cement at low curing temperature, Constr. Build. Mater. 408 (2023). https://doi.org/10.1016/j.conbuildmat.2023.133779.

[54] X. Chen, S. Wei, Q. Wang, M. Tang, X. Shen, X. Zou, Y. Shen, B. Ma, Morphology prediction of portlandite: Atomistic simulations and experimental research, Appl. Surf. Sci. 502 (2020). https://doi.org/10.1016/j.apsusc.2019.144296.

[55] B. Zeng, Z. Zhang, S. Yang, L. Mo, F. Jin, Alkanolamines-activated steel slag for stabilization/solidification of heavy metal contaminated soil, J. Environ. Chem. Eng. 11 (2023) 110301. https://doi.org/10.1016/j.jece.2023.110301.

[56] A. V. Soin, L.J.J. Catalan, S.D. Kinrade, A combined QXRD/TG method to quantify the phase composition of hydrated Portland cements, Cem. Concr. Res. 48 (2013). https://doi.org/10.1016/j.cemconres.2013.02.007 .

[57] J. Wang, J. Liao, X. Kong, J. Yin, Characterization of the nanoparticles formed in aqueous phase of hydrating cement pastes in the presence of PCEs, Cem. Concr. Res. 165 (2023). https://doi.org/10.1016/j.cemconres.2022.107087.

[58] P.J. Williams, J.J. Biernacki, J. Bai, C.J. Rawn, Assessment of a synchrotron X-ray method for quantitative analysis of calcium hydroxide, Cem. Concr. Res. 33 (2003). https://doi.org/10.1016/S0008-8846(03)00105-4.

[59] Y.A. Villagrán-Zaccardi, H. Egüez-Alava, K. De Buysser, E. Gruyaert, N. De Belie, Calibrated quantitative thermogravimetric analysis for the determination of portlandite and calcite content in hydrated cementitious systems, Mater. Struct. 50 (2017) 179. https://doi.org/10.1617/s11527-017-1046-2.

[60] Y. Zhang, X. Zhang, X. Cai, L. Gao, Q. Li, X. Kong, A further understanding on the strength development of cement pastes in the presence of triisopropanolamine used in CRTS III slab track, Constr. Build. Mater. 315 (2022). https://doi.org/10.1016/j.conbuildmat.2021.125743.

[61] E. John, B. Lothenbach, Cement hydration mechanisms through time – a review, J. Mater. Sci. 58 (2023). https://doi.org/10.1007/s10853-023-08651-9.

[62] C. Rodriguez-Navarro, E. Ruiz-Agudo, A. Burgos-Cara, K. Elert, E.F. Hansen, Crystallization and colloidal stabilization of Ca(OH)2 in the presence of nopal juice (Opuntia ficus indica): Implications in architectural heritage conservation, Langmuir 33 (2017). https://doi.org/10.1021/acs.langmuir.7b02423.

[63] K. Riding, D.A. Silva, K. Scrivener, Early age strength enhancement of blended cement systems by CaCl2 and diethanol-isopropanolamine, Cem. Concr. Res. 40 (2010) 935–946. https://doi.org/10.1016/j.cemconres.2010.01.008.

[64] E. Gallucci, K. Scrivener, Crystallisation of calcium hydroxide in early age model and ordinary cementitious systems, Cem. Concr. Res. 37 (2007). https://doi.org/10.1016/j.cemconres.2007.01.001.

[65] A. Setiawan, Simulation of interfaces in construction materials: tricalcium silicate, gypsum, and organic modifiers, Экономика Региона (2012).

[66] A.A. Naiini, J. Pinkas, W. Plass, V.G. Young, J.G. Verkade, Triethanolamine complexes of H+, Li+, Na+, Sr2+, and Ba2+ Perchlorates, Inorg. Chem. 33 (1994). https://doi.org/10.1021/ic00088a014.

[67] Y. Zhao, Y. Chen, X. Li, D. Chen, M. Wu, The use of TEA·H3PO4 and TEA·C18H30O3S as eco-friendly corrosion inhibitors in cementitious materials: An experimental and theoretical study, Cem. Concr. Res. 165 (2023). https://doi.org/10.1016/j.cemconres.2022.107073.

[68] G. Chauhan, M. Stein, A. Seidel-Morgenstern, K.K. Pant, K.D.P. Nigam, The thermodynamics and biodegradability of chelating agents upon metal extraction, Chem. Eng. Sci. 137 (2015). https://doi.org/10.1016/j.ces.2015.07.028

Figure Captions

Fig. 1. The XRD diffractograms of raw materials.